Piezo mediates Rho activation and actin stress fibre formation in *Drosophila* nephrocytes

Kristina Schulz [1,2], Ilka Edenhofer [1,2], Maja Lindenmeyer [1,2], Christian Lohr [4], Tobias B. Huber [1,2], Barry Denholm [3] and Sybille Koehler [1,2,3]

[1] III. Department of Medicine, University Medical Center Hamburg-Eppendorf, Hamburg, Germany; [2] Hamburg Center for Kidney Health (HCKH), University Medical Center Hamburg-Eppendorf, Hamburg, Germany; [3] Biomedical Sciences, University of Edinburgh, Edinburgh, Scotland, UK; [4] Division of Neurophysiology, Institute of Cell and Systems Biology of Animals, University of Hamburg, Hamburg, Germany

Corresponding author:

Sybille Koehler

Campus Forschung N27
Martinistraße 52
UKE Hamburg
20246 Hamburg
Germany

Sy.koehler@uke.de

Running title: Piezo mediates Rho activation in nephrocytes

Keywords: Drosophila, Nephrocyte, Mechanosensation, glomerular disease, GTPase, actin-cytoskeleton

Abstract

Due to their position on glomerular capillaries, podocytes are continuously counteracting biomechanical filtration forces. Most therapeutic interventions known to generally slow or prevent the progression of chronic kidney disease appear to lower the biochemical forces on podocytes, highlighting the critical need to better understand podocyte mechano-signalling pathways. Here we investigated the hypothesis that the mechanotransducer Piezo is involved in a mechanosensation pathway in *Drosophila* nephrocytes, the podocyte homologue in the fly. Our data show Piezo is expressed in nephrocytes where it localises to the nephrocyte diaphragm. Further, the Piezo agonist Yoda1 caused a significant increase of intracellular Ca^{++} upon exposure to mechanical force in nephrocytes. Loss of function analysis in Piezo knockout nephrocytes revealed only mild defects in nephrocyte function. Further, we show that elevated Piezo expression levels resulted in constitutive Ca^{++} oscillations, Rho1 hyperactivity and accumulation of actin stress fibres, culminating in a severe nephrocyte phenotype, suggesting that pathway hyperactivity is detrimental. Interestingly, expression of Piezo, which lacks mechanosensitive channel activity, did not result in a severe nephrocyte phenotype and activation of Rho1 suggesting the observed changes in Piezo wildtype overexpressing cells are caused by the mechanosensitive channel activity. Moreover, blocking Piezo activity using the tarantula toxin GsMTx4 reduced Rho1 hyper-activation in nephrocytes overexpressing Piezo. Taken together, these data show that Piezo plays an important role in nephrocyte mechanotransduction but that its activity need to be kept within bounds.

Introduction

Kidney podocytes are highly specialized epithelial cells, which together with the fenestrated endothelium and the glomerular basement membrane, constitute the three-layered, size and charge selective filter of the glomerular filtration barrier [1]. Podocytes have a unique morphology, forming primary and secondary foot processes which completely enwrap the capillaries. Injury to podocytes causes severe morphological change, detachment from the basement membrane and finally loss of podocytes into the primary urine. Several genes are known to be important for podocyte biology, among them are NPHS1, NPHS2, TRPC6 and Actinin-4 [2–6]. Loss of podocytes has pathological consequences as these cells are post-mitotic and cannot be replenished. The blank capillaries are not sealed anymore, resulting in massive loss of protein from blood into urine, so called proteinuria. Podocyte injury can occur because of genetic deficiencies [2–6], toxin-mediated triggers [7] and changes in the physical environment within the glomerulus [8–11].

Podocytes are under constant mechanical force and regularly face changes in these forces, as they are responsible for the filtration of ~180 litres of primary urine each day. The main forces arising from this are hydrostatic pressure (50 kPa) and fluid shear stress at the filtration slits (8 Pa) [12]. These forces increase during diseases such as diabetes and hypertension and result in podocyte loss [10]. Progressive loss of podocytes leads to a vicious cycle, as biomechanical forces experienced by those cells remaining, increase further. It is known, that remaining podocytes respond by growing in size to re-cover the blank capillary to overcome the challenge originating from loss of neighbouring cells; this is considered to be an adaptive and protective mechanism [13–15]. In order for this to happen, podocytes must exhibit mechanotransductive mechanisms to recognize these changes in the physical environment and initiate

adaptive and protective responses, likely candidates are TRPC6, YAP, Talin, Filamins and Piezo [5,8,9,16–19].

Piezo is a mechanosensitive ion channel that is involved in mechanotransduction in many developmental and physiological contexts. Piezo channels (Piezo1 and Piezo2) open in response to mechanical force and allow the influx of positively charged ions such as Ca^{++} and Na^{+} [20,21]. The two proteins have different functional roles as Piezo1 was reported to be essential for sensing blood flow-associated shear stress and blood vessel development [22–24], while Piezo2 responds to touch and proprioception [25].

Whether Piezo plays a role in mechanotransduction in nephrocytes, the podocyte homologue in flies, is unknown. To address these questions, we investigated the effect of Piezo depletion and activation on nephrocyte morphology and function. Nephrocytes form invaginations of the plasma membrane, which resemble foot processes and are spanned by the nephrocyte diaphragm, a highly-specialized cell-cell contact, that is highly similar to the mammalian podocyte slit diaphragm [26,27]. They function as filtration units in the fly and filter toxins and waste products from the haemolymph. Our data shows that the mechanotransducer Piezo is expressed in nephrocytes and localizes to the nephrocyte diaphragm. In nephrocytes, Piezo loss of function results in a relatively mild functional phenotype, whereas overexpression of Piezo results in a severe nephrocyte phenotype, Rho1 hyperactivity and accumulation of actin stress fibres. These data show that Piezo is a mechanotransducer in nephrocytes and reveal its expression levels have to be regulated.

Results

Piezo is expressed in nephrocytes and localizes to the nephrocyte diaphragm

To investigate the functional role of Piezo and the effect of altered expression levels of the mechanotransducer, we utilized the *Drosophila* nephrocyte model. Piezo expression has not been studied in nephrocytes before. We find Piezo is expressed in nephrocytes, where it localises closely to the nephrocyte diaphragm protein Dumbfounded (Duf), the NEPH homolog in the fly [Pearson's correlation coefficient (PCCs): 0,5042 (adult) and 0,4621 (larvae)] **(Figure 1A,B,C; Supp. Figure 1E)**. PCCs above 0.4 are considered moderate positive correlations [28], hence the calculated values for Duf and Piezo show that both proteins partially overlap. The co-localisation of Piezo with Polychaetoid (Pyd) was (significantly) less, in comparison (Pearson's correlation coefficient: 0,3496 (adult) and 0,3589 (larvae)) **(Figure 1B,C; Supp. Figure 1E)**. As the PCCs for Pyd and Piezo are below 0.4 they can be considered as weak positive correlation, suggesting that Piezo localises closer to the nephrocyte diaphragm protein Duf and might be part of the protein complex associated with the nephrocyte diaphragm. However, biochemical interaction data is elusive. These data show Piezo localises to or close to the nephrocyte diaphragm complex and hence would be in a good position to monitor forces across the filtration diaphragm.

In the next step, we wanted to confirm functionality of the channel in nephrocytes. To do so, we used Yoda1, which is a chemical compound that specifically facilitates Piezo opening at lower magnitude of force [29,30]. As Piezo is a Ca^{++} permeable cation channel and known to be important for Ca^{++} influx, we investigated the effect of Yoda1 by measuring Ca^{++} levels in nephrocytes. Piezo channels are sensitive to mechanical stimuli and stretch. Therefore, we applied a pressure stimulus ('puff') to the tissue to induce mechanical stress in nephrocytes and elicit Piezo-mediated Ca^{++} signaling. In detail, a glass micropipette, either filled with Yoda1 (30 µM) or DMSO

(control, equal amount to Yoda1), was positioned on the bath solution's surface and pulled with a patch-pipette puller with an electrical resistance of 200-300 kΩ. The puff, and therefore the release of liquid in a controlled way, causes a mechanical stimulus, which resembles shear stress.

Nephrocytes were incubated with Yoda1 or DMSO (control) for 5 mins prior to measuring Ca^{++} by imaging GCaMP6 signal. After imaging for 60 secs, we applied a puff of 0.2 bar for 3 secs, which resulted in an increase of GCaMP6 intensity in nephrocytes. Quantification of this increase revealed a significantly higher magnitude of GCaMP6 intensity after Yoda1 incubation when compared to DMSO control **(Figure 1D)**. Of note, for the majority of flies pre-treated with Yoda1, Ca^{++} levels did not return to baseline within the 340 secs timeframe of the recordings. This data suggests, that pharmacological activation of Piezo by Yoda1 caused an elevated influx of Ca^{++} after applying mechanical force to nephrocytes and that Yoda1 facilitates opening of Piezo in nephrocytes.

Piezo2 has recently been described to be expressed in renin-producing cells of the juxta-glomerular apparatus and mesangial cells in the kidney [31,32].

We further examined Piezo1 expression in mammalian tissue. A previous study revealed Piezo1 expression in mouse glomeruli [19], and proteomic analysis of isolated murine podocytes, revealed expression of Piezo1 (12.25% enrichment when compared to non-podocyte glomerular cells) [33], strengthening support for our hypothesis that Piezo1 is a mechanotransducer in the mammalian podocytes as well. We examined expression of Piezo1 in mammalian glomeruli, by co-staining with the podocyte marker Synaptopodin and found Piezo1 expression in podocytes **(Supp. Figure 1B)**. Investigating publicly available single nucleus RNA-sequencing data for mouse and human kidney, revealed expression of Piezo1 in podocytes as well **(Supp. Figure 1C,D)** [34,35]. Moreover, searching Piezo1 in the single cell RNA-sequencing data

from the Kidney Precision Medicine Project revealed expression of the channel in healthy controls and patients suffering from CKD.

Taken together, the data provided here, confirm expression of Piezo in nephrocytes, localising to the nephrocyte diaphragm, and its involvement in Ca^{++} influx after applying force.

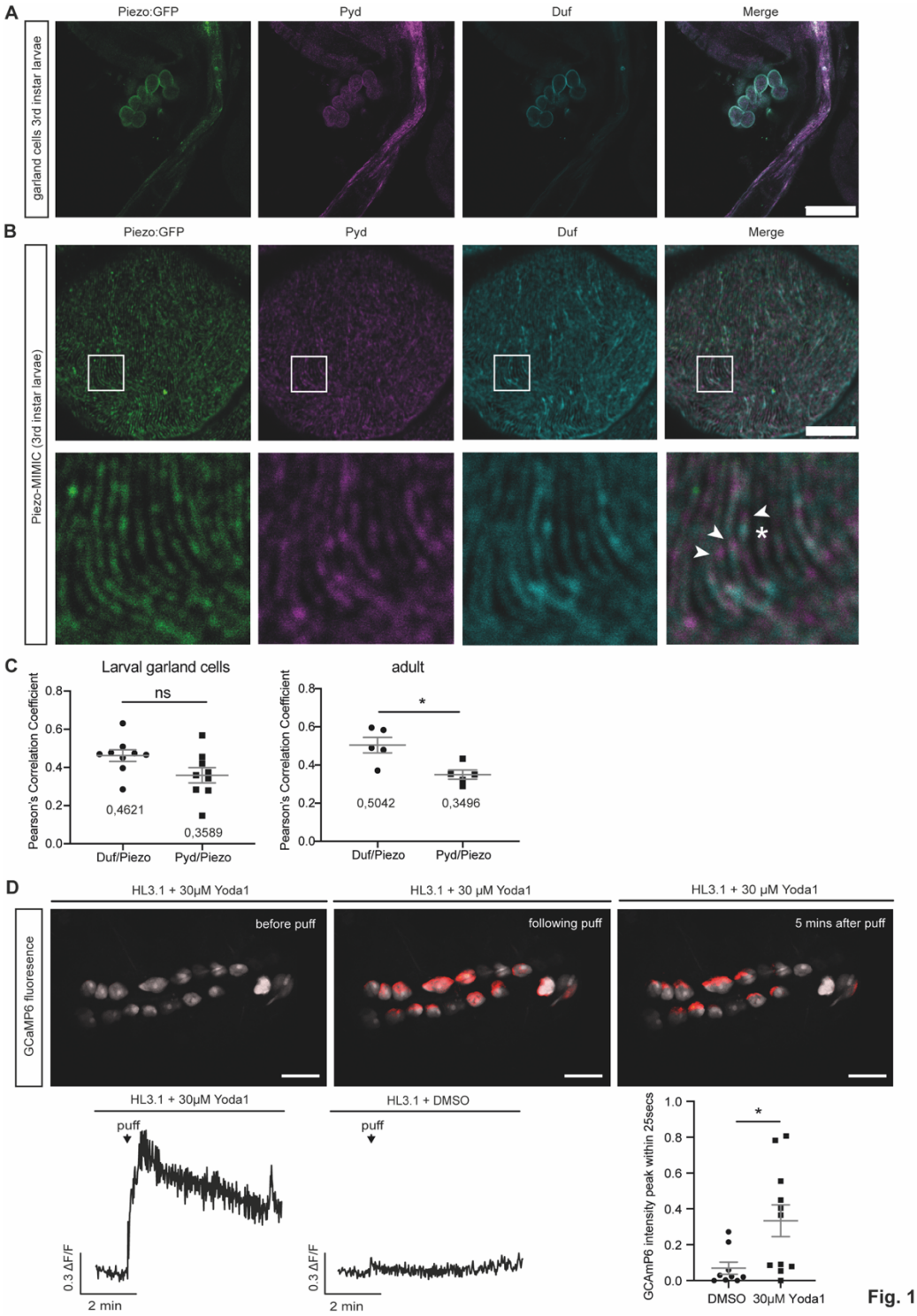

Fig. 1

Figure 1: Piezo is expressed in nephrocytes and localizes to the nephrocyte diaphragm. A Immunofluorescence staining with a Duf (dNEPH) and Pyd (dZO1) antibody revealed expression and localisation of Piezo (Piezo:GFP; Mi{MIC} line) at the nephrocyte diaphragm in garland nephrocytes from 3rd instar larvae . Scale bar = 50 μm. **B** High resolution microscopy showed expression of Piezo in close proximity to the nephrocyte diaphragm protein Duf, the NEPH homologue, and Pyd in garland larval nephrocytes. Scale bar = 5 μm. **C** Calculation of the Pearson's correlation coefficient revealed a higher degree of co-localisation of Piezo with Duf in both cell types. Student's t-test: *: $p < 0.05$. **D** Images display fluorescent recordings of calcium signals (red) under baseline conditions (left), induced by mechanical force (middle), and 5 mins after the force stimulus (right). Cells were treated with Yoda1 for 5 mins prior to the measurement. The corresponding trace is shown below (left) in comparison to a recording of cells without prior Yoda1 treatment (middle). Yoda1-treated cells present with a significant increase of GCaMP6 intensity after applying force when compared to DMSO-treated control cells (right). Student's t-test: *: $p < 0.05$. w; *sns*-Gal4/+;UAS-*dicer2*/UAS-*GCaMP6m*. Scale bar = 20 μm.

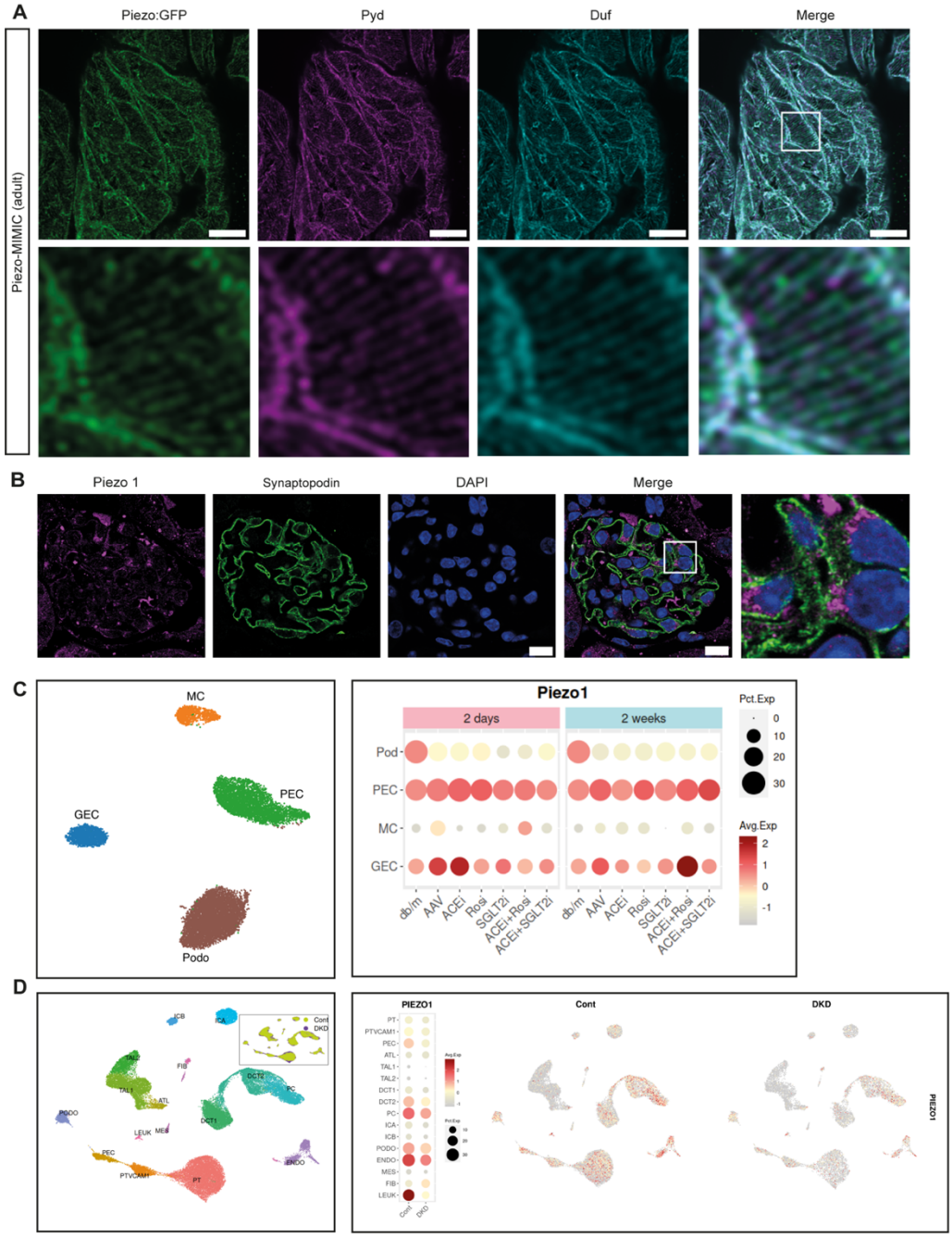

Supp. Fig. 1

Supp. Figure 1: Expression of Piezo in pericardial nephrocytes. A Immunofluorescence visualizing the nephrocyte diaphragm with Pyd and Duf revealed expression and localisation of Piezo (Piezo:GFP; Mi{MIC} line) at the nephrocyte diaphragm in adult pericardial cells. Scale bar = 50 μm. **B** Piezo1 is expressed in mammalian podocytes, which are visualized using the podocyte marker Synaptopodin. Scale bar = 10 μm. **C** Single nucleus RNA-sequencing data from diabetic mouse models. Data is available online from the Humphries lab (usage with permission) [34]. Piezo1 is expressed in glomeruli, but not exclusively in podocytes. **D** Single nucleus and ATAC-sequencing data from human diabetic kidney disease samples and controls revealed Piezo1 expression in podocytes. Data used from the Humphries lab with permission [35].

Loss of Piezo results in a mild functional nephrocyte phenotype

After the expression of Piezo in nephrocytes was confirmed, we wanted to know if Piezo is important for nephrocyte morphology and function, and whether altered expression levels impact on nephrocyte biology. To address this question, we first examined nephrocyte diaphragm morphology and filtration function in animals completely lacking Piezo ($Piezo^{KO}$). Loss of Piezo did not result in changes to nephrocyte diaphragm integrity as assessed by immunofluorescence **(Figure 2A,B)**. FITC-Albumin binding assays revealed a significant increase of FITC-Albumin binding after depletion of Piezo (whole body knockout). In line with this, nephrocyte-specific depletion of Piezo induced by RNAi knock-down revealed a trend towards more FITC-Albumin binding, although this did not reach significance **(Figure 2C)**.

However, the FITC-Albumin assay cannot distinguish between uptake, filtration and endocytosis. To assess the effect of Piezo depletion on filtration function in the context of nephrocyte function to remove toxins from the haemolymph, we performed the $AgNO_3$ toxin assay [26]. Nephrocytes are important to clear the haemolymph from toxins and waste products to ensure normal growth and development. $AgNO_3$ is a toxin which, when fed to larvae, accumulates in the haemolypmh and retards normal development; nephrocytes are able to counteract this by clearing $AgNO_3$ from the circulation [26]. Impaired nephrocyte function results in less clearance resulting in a delay of larval pupation. As the $Piezo^{KO}$ lesion is in a w^{1118} background ($Piezo^{KO}$ was

backcrossed into w^{1118} for six generations prior to experiments), we used this strain as a control for the $Piezo^{KO}$. Interestingly, the w^{1118} strain presented with a delayed pupation, which was similar to the $Piezo^{KO}$, suggesting that the filtration defect is not caused by depletion of Piezo, but rather due to the genetic background **(Figure 2D)**. To further confirm, that loss of Piezo does not influence filtration function and therefore pupation, we also used a Piezo-RNAi fly strain to deplete Piezo only in nephrocytes and could show, that a knockdown of Piezo also did not reveal any differences in pupation when compared to control flies **(Figure 2E)**. As only FITC-Albumin binding was altered upon loss of Piezo, but $AgNO_3$ clearance was not changed, we conclude that Piezo depletion only causes a mild functional phenotype and filtration is not severely hampered.

Our data shows that loss of Piezo results only in increased FITC-Albumin binding, but does not impact nephrocyte diaphragm morphology.

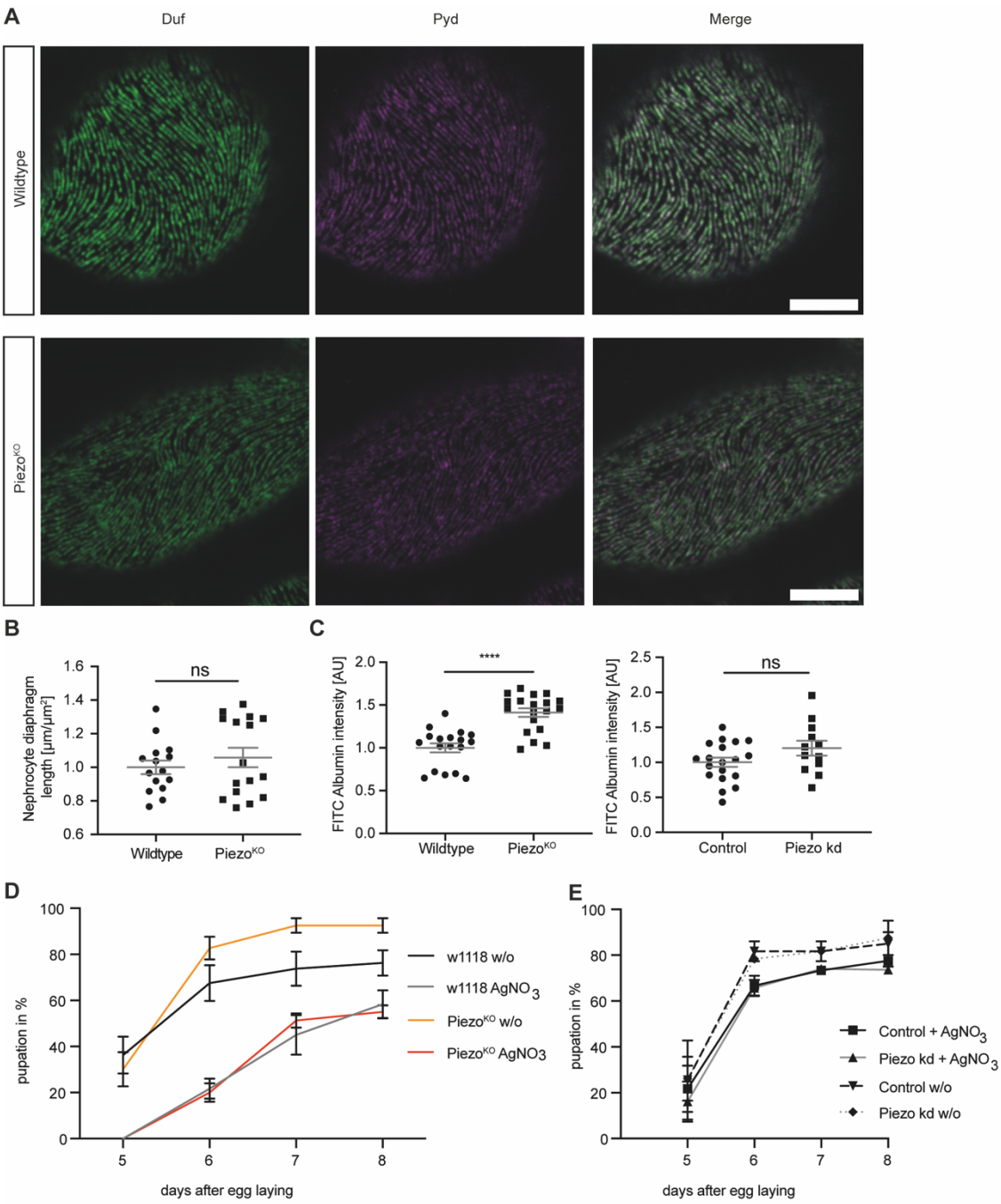

Fig. 2

Figure 2: Loss of Piezo caused a mild functional nephrocyte phenotype. A,B Immunofluorescence staining with a Duf and Pyd antibody did not reveal any morphological changes in Piezo^{KO} (w;+;*piezo*^{ko}) nephrocytes in comparison to control cells (wildtype w^{1118}). Scale bar 5 = µm. **C** FITC-Albumin binding assays revealed a functional defect with an increased FITC-Albumin binding in Piezo^{KO} nephrocytes, while nephrocyte specific depletion of Piezo did not result in significant changes. Student's t-test: ****: $p < 0.0001$. Control: w;*sns*-Gal4/+;UAS-*dicer2*/+; Piezo kd: w;*sns*-Gal4/ UAS-*piezo*-RNAi;UAS-*dicer2*/+. **D** $AgNO_3$ toxin assays did not reveal a filtration defect, as Piezo^{KO} flies showed a similar delay in pupation when compared to controls (wildtype w1118). **E** $AgNO_3$ toxin assay using Piezo RNAi also did not reveal any differences in pupation behaviour, when compared to control flies.

Elevation of Piezo levels caused a severe nephrocyte phenotype, significantly increased Rho1-GTP levels and actin stress fibre formation

Depletion of Piezo by knockout revealed only a mild phenotype with an increase in FITC-Albumin binding, but no impact on $AgNO_3$ clearance or nephrocyte morphology. Hence, we further investigated whether an overexpression of the channel results in a nephrocyte phenotype. First, we analysed the impact of increased Piezo levels on nephrocyte morphology and function. The UAS-Gal4 system is influenced by temperature, being more active at a higher temperature. We used two different temperatures (medium: 25°C and high: 28°C) for Piezo overexpression.

Our data show nephrocyte diaphragm morphology was not impacted by Piezo overexpression at medium levels, but at high levels resulted in a significant reduction of nephrocyte diaphragm density **(Figure 3A,B; Supp. Figure 2A,B,D,E)**. Our findings suggest that the elevated levels of Piezo are detrimental for nephrocyte morphology, at least at high expression levels. FITC-Albumin binding was significantly increased in cells expressing high levels of Piezo wildtype when compared to control cells (both kept at 28°C) **(Figure 3C)**. In line with the FITC-Albumin binding assay data, the $AgNO_3$ toxin assay revealed a severe filtration defect already at 25°C, with a significant delay of pupation detectable from day 5 in flies expressing Piezo wildtype in nephrocytes **(Figure 3D)**. Additional controls, which express GFP in nephrocytes did not present with delayed pupation **(Figure 3E)**.

Ca^{++} is a second messenger in cells and can act by modulating GTPase activation. It is known that over-activation of the GTPases RhoA and Rac1 results in podocyte injury in mice [36–38]. Hence, we measured the localisation and cortical intensity of GTP-bound Rho1 in nephrocytes overexpressing Piezo wildtype and respective controls to determine if these might be downstream components of the pathway. We used Rok-RBD (a Rho1 sensor binding to GTP-bound Rho1) to visualize active Rho1

in nephrocytes. This revealed a significant increase of Rho1-activity at the cell cortex in Piezo wildtype expressing cells **(Figure 3F)**. In addition, interfering with Rho1 activation by simultaneous expression of a dominant-negative variant of Rho1 in Piezo wildtype overexpressing cells, resulted in a rescue of the FITC-Albumin binding phenotype **(Figure 3G)**. This suggests that the functional phenotype observed in Piezo overexpression nephrocytes is at least partially mediated via aberrant Rho1 activation. As activation of Rho1 was described to cause actin stress fibre formation in podocytes [39], we visualized the actin cytoskeleton with LifeAct-RFP. In addition, previous work revealed the presence of cortical stress fibres and actin clusters in *Drosophila* nephrocytes [40]. In line with the activation of Rho1, overexpression of Piezo wildtype caused a significant increase of both, cortical actin fibres and actin clusters, when compared to controls **(Figure 3H)**. Our data shows that Piezo wildtype overexpression causes a severe nephrocyte phenotype, including altered morphology and function, and resulted in increased active Rho1 levels at the cell cortex and increased actin stress fibres.

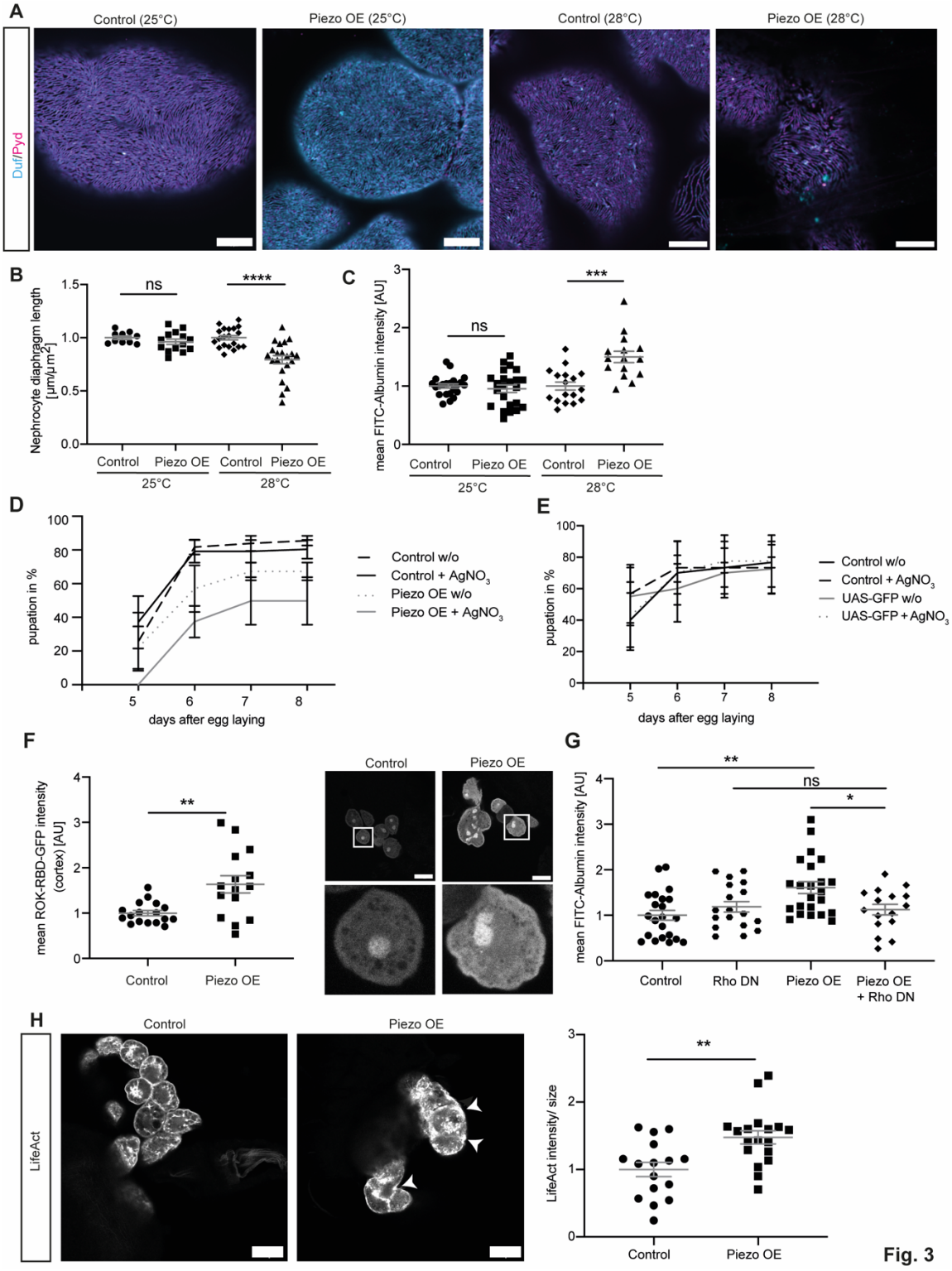

Figure 3: Elevated Piezo levels cause a nephrocyte phenotype and result in elevated Rho1-GTP levels and more actin stress fibres. A,B Immunofluorescence staining with a Duf (cyan) and Pyd (magenta) antibody did not reveal any morphological changes in nephrocytes expressing Piezo wildtype at 25°C, while flies kept at 28°C showed a significant reduction in nephrocyte diaphragm density (**B**). Student's t-test: ****: $p < 0.0001$. Scale bar = 5µm. Control: w; *sns*-Gal4/+;UAS-*dicer2*/+. Piezo OE: w; *sns*-Gal4/+;UAS-*dicer2*/UAS-*piezo*-GFP. **C** FITC-Albumin assays revealed a significantly increased FITC-Albumin binding in nephrocytes expressing Piezo wildtype at 28°C, while no filtration defect was observed at 25°C. Student's t-test: ***: $p < 0.001$. **D** $AgNO_3$ toxin assays confirmed a severe filtration defect, as larvae expressing Piezo wildtype in nephrocytes present with a significantly delayed pupation

behaviour already at 25°C. 2way-ANOVA with Tukey's multiple comparison test: *: $p < 0.05$. **E** $AgNO_3$ toxin assays showing no delay in pupation caused by GFP expression in nephrocytes. **F** Expression of Piezo wildtype caused a significant increase of GTP-bound Rho1 levels at the cell cortex. Student's t-test: **: $p < 0.01$. control: w; *sns*-Gal4/+;UAS-*rok-RBD-GFP*/+; Piezo OE: w; *sns*-Gal4/+;UAS-*rok-RBD-GFP*/UAS-*piezo*-flag. **G** Simultaneous expression of Piezo wildtype with dominant-negative Rho1 resulted in a significant decrease of FITC-Albumin binding when compared to Piezo wildtype overexpression (Piezo OE). Expression of Rho-DN alone did not impact on FITC-Albumin binding. 1way-ANOVA with Tukey's multiple comparison test: *: $p < 0.05$; **: $p < 0.01$. control: w; *sns*-Gal4/+;UAS-*dicer2*/+; Rho-DN: w; *sns*-Gal4/+;UAS-*dicer2*/UAS.*rho1.N19*; Piezo OE: w; *sns*-Gal4/+; UAS-*piezo*-GFP/+; Piezo OE + Rho-DN: w; *sns*-Gal4/+; UAS.*rho1.N19*/UAS-*piezo*-GFP. **H** Visualisation of the actin cytoskeleton revealed an increase of cortical actin stress fibers (arrow heads) and actin clusters in nephrocytes expressing Piezo wildtype. Quantification was done for the whole cell. Student's t-test: **: $p < 0.01$. Scale bar = 25μm. Control: w; *sns*-Gal4/+;UAS-*LifeACT*-RFP/+. Piezo OE: w; *sns*-Gal4/+;UAS-*LifeACT*-RFP/UAS-*piezo*-GFP.

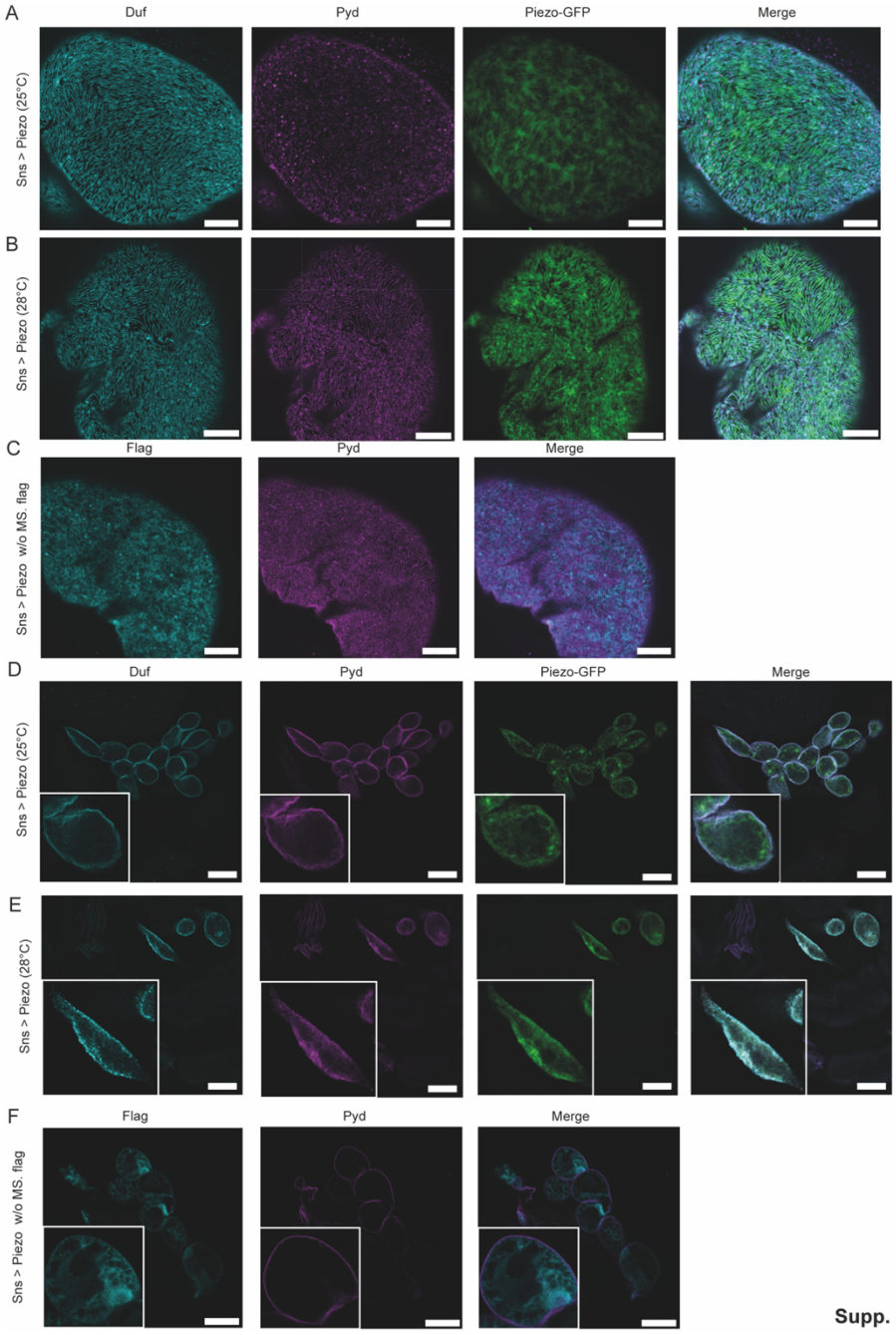

Supp. Fig. 2

Supp. Figure 2: Piezo overexpression and localisation in nephrocytes. A,D Nephrocytes expressed Piezo-GFP at 25°C, which localizes to the cell cortex and the lacunae. Scale bar = 5μm (A); scale bar = 25μm (D). **B,E** Piezo-GFP expression at 28°C revealed expression and localisation to the cell cortex as well as the lacunae channels. Scale bar = 5μm (B); scale bar = 25μm (E). **C,F** Expression of Piezo lacking mechanosensation channel activity (Piezo w/o MS) revealed expression and localisation of the channel at the cell cortex and extended into the lacunae system. Scale bar = 5μm (C); scale bar = 25μm (F).

The mechanosensation domain of Piezo is important for Rho1 GTPase activation

While Piezo depletion only exhibits a mild phenotype, elevated levels caused a severe nephrocyte phenotype including increased Rho1-GTP levels at the cell cortex. Piezo is a Ca^{++} permeable cation channel and force induced opening of the channel results in increased intracellular Ca^{++} levels [41]. To further investigate the functional role of the mechanosensitive domain in nephrocytes, we used a fly strain expressing a Piezo mutant lacking the mechanosensitive channel activity (Piezo w/o MS; UAS-*piezo*.2306MYC.flag) [42].

First, we assessed Ca^{++} influx in Piezo wildtype overexpressing cells. Interestingly, even without any biomechanical force applied, overexpression of Piezo wildtype resulted in an oscillating Ca^{++} signalling pattern in the majority of flies investigated (62.5%). This spontaneous oscillating pattern was significantly less in control flies (20%) and flies expressing a Piezo mutant lacking the mechanosensitive channel activity (Piezo w/o MS) (22.2%) **(Figure 4A,B)**. We also applied mechanical force by using a mechanical stimulus (puff), however, the presence of oscillation in Piezo wildtype cells posed a challenge in quantifying the post-force increase, as it became indistinguishable from the oscillation. Since nephrocytes expressing the mutant Piezo variant lacking mechanosensitive channel activity exhibit an oscillatory pattern in only a limited number of flies (22.2%), it suggests that the oscillations are enhanced by the mechanosensitive activity of Piezo.

Based on our finding that the lack of the mechanosensitive channel activity seems to change intracellular Ca^{++} levels, we further investigated nephrocyte morphology and function in flies expressing Piezo w/o MS.

Immunofluorescence imaging revealed a significant increase of nephrocyte diaphragm density at medium levels **(Figure 4C,D; Supp. Figure 2C,F)**. Nephrocyte morphology at high expression levels however was unaffected, which is in contrast to the wildtype data, suggesting that this phenotype is based on its mechanosensitive channel activity, at least at high expression levels. FITC-Albumin binding assays did not reveal any differences in FITC-Albumin binding at medium or high expression levels **(Figure 4E)**.

Interestingly, nephrocytes expressing the mutant version of Piezo without the mechanosensitive channel activity, did not present with elevated Rho1-GTP levels at the cell cortex when compared to controls, suggesting the mechanosensitive function of Piezo is involved in Rho1-GTPase activation **(Figure 4F)**. Our data shows that Piezo overexpression causes a severe nephrocyte phenotype, including altered morphology and function, and resulted in increased active Rho1 levels at the cell cortex and increased actin stress fibres. This phenotype seems to be mediated by its mechanosensitive channel activity, as the Piezo mutant lacking mechanosensitive channel activity did not cause a functional phenotype, nor Rho1-GTPase activation.

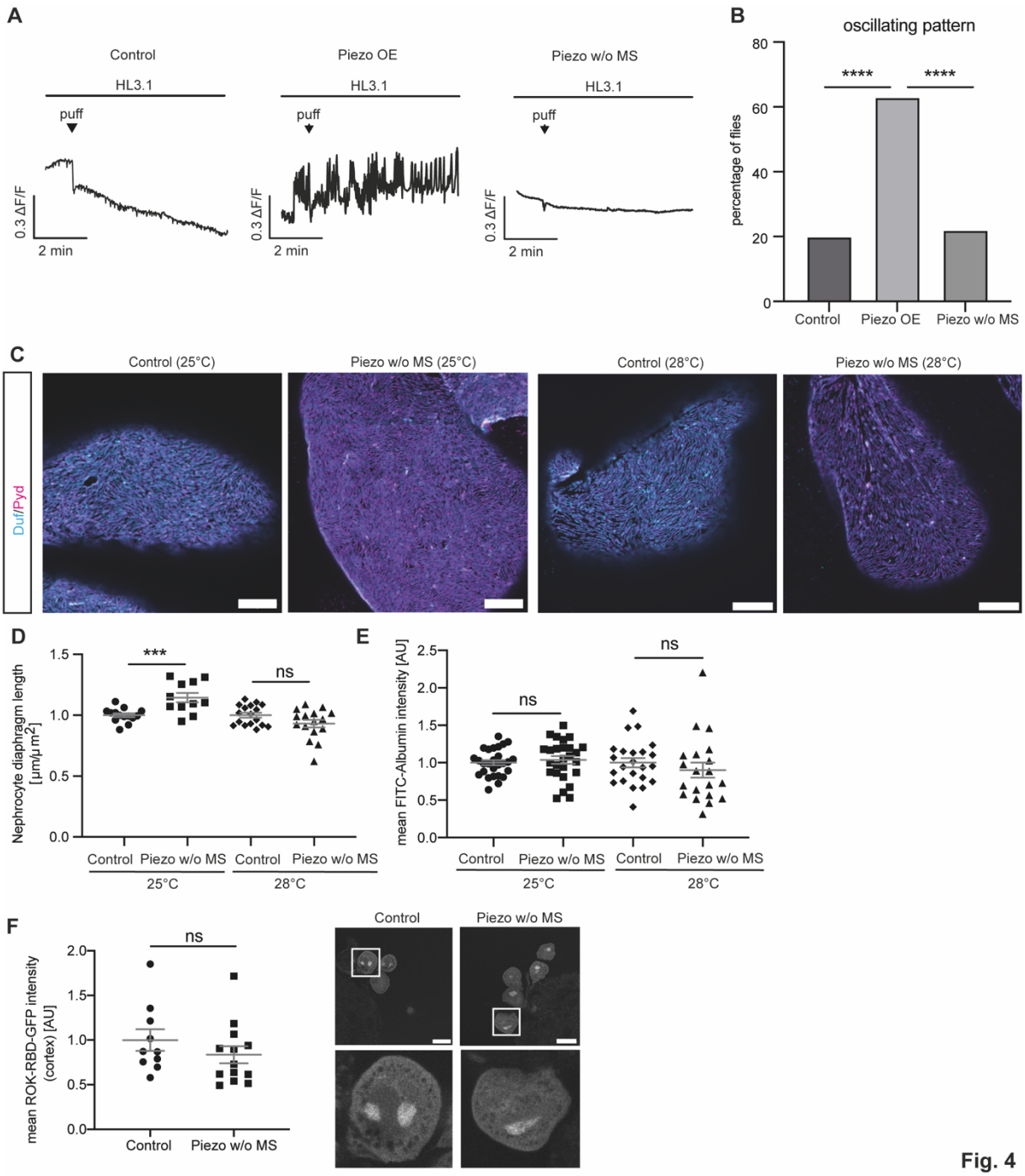

Fig. 4

Figure 4: Elevated Piezo levels cause oscillating Ca^{++} signals and the mechanosensitive channel activity seems to be important for Rho1 activation. A Traces of Ca^{++} signals of nephrocytes in control flies (left), in flies expressing GCaMP6 and Piezo wildtype (overexpression) (middle), and in flies expressing Piezo without mechanosensitive channel activity (right). Control: w; *sns*-Gal4/+;UAS-*GCaMP6m*/+; Piezo OE: w; *sns*-Gal4/+;UAS-*GCaMP6m*/UAS-*piezo*-flag; Piezo w/o MS: w; *sns*-Gal4/+;UAS-*GCaMP6m*/UAS-*piezo*-2306MYC.flag. **B** Analysis of calcium event patterns revealed a significant oscillatory trend in the majority of flies overexpressing Piezo wildtype, whereas this could only be observed in a limited number of flies among controls and those overexpressing Piezo without mechanosensitive channel activity. Chi-square test: ****: $p < 0.0001$. Number of flies: Control: 10; Piezo OE: 8; Piezo w/o MS: 9. **C,D** Immunofluorescence staining with a Duf (cyan) and Pyd (magenta) antibody did reveal a significant increase of nephrocyte diaphragm density in flies expressing Piezo w/o MS at 25°C, while no difference could be observed at 28°C. (**D**) Student's t-test: ***: $p < 0.001$. Scale bar = 5µm. Control: w; *sns*-Gal4/+;UAS-*dicer2*/+, Piezo w/o MS: w; *sns*-Gal4/+;UAS-*GCaMP6m*/UAS-

piezo-2306MYC.flag. **E** FITC-Albumin assays did not reveal altered FITC-Albumin binding at 25°C or 28°C. **F** Nephrocytes expressing Piezo without the mechanosensitive channel activity did not reveal an accumulation of active Rho1 at the cell cortex when compared to controls. Student's t-test. control: w; *sns*-Gal4/+;UAS-*rok-RBD-GFP*/+; Piezo w/o MS: w; *sns*-Gal4/+;UAS-*rok-RBD-GFP*/UAS-*piezo*-2306MYC.flag.

Pharmacological inhibition with tarantula toxin reduced the elevated Rho1-GTP levels in Piezo overexpressing cells

Overexpression of Piezo resulted in a severe nephrocyte phenotype including morphological and functional disturbances, significantly increased Rho1-GTP levels and more actin stress fibres and clusters. Therefore, we tested whether pharmacological inhibition of the channel could reverse the phenotype and be beneficial for nephrocyte function. To do so, we used tarantula toxin (GsMTx4), which integrates into the cell membrane and blocks the opening of the channel upon mechanical stretch [43] . Of note, GsMTx4 is not specific for inhibiting Piezo, but also acts on other cation channels.

Acute inhibition of the mechanosensitive channel with GsMTx4 did not result in nephrocyte diaphragm morphological or functional disturbances **(Figure 5A,B)**. GTPases assessment and analysis of the actin cytoskeleton also did not reveal significant differences in comparison to control cells **(Figure 5C,D,E)**. Overexpression of Piezo caused a significant increase of GTP-bound Rho1 levels at the cell cortex, hence we treated the Piezo overexpression nephrocytes with GsMTx4 and quantified Rho1 activity levels at the cortex. 5 min treatment with the toxin significantly reduced the Rho1 activity levels in Piezo overexpression nephrocytes **(Figure 5F).**

Taken together, a treatment with the toxin did not reveal severe pathological effects on nephrocyte morphology and function and might therefore be a potential novel intervention.

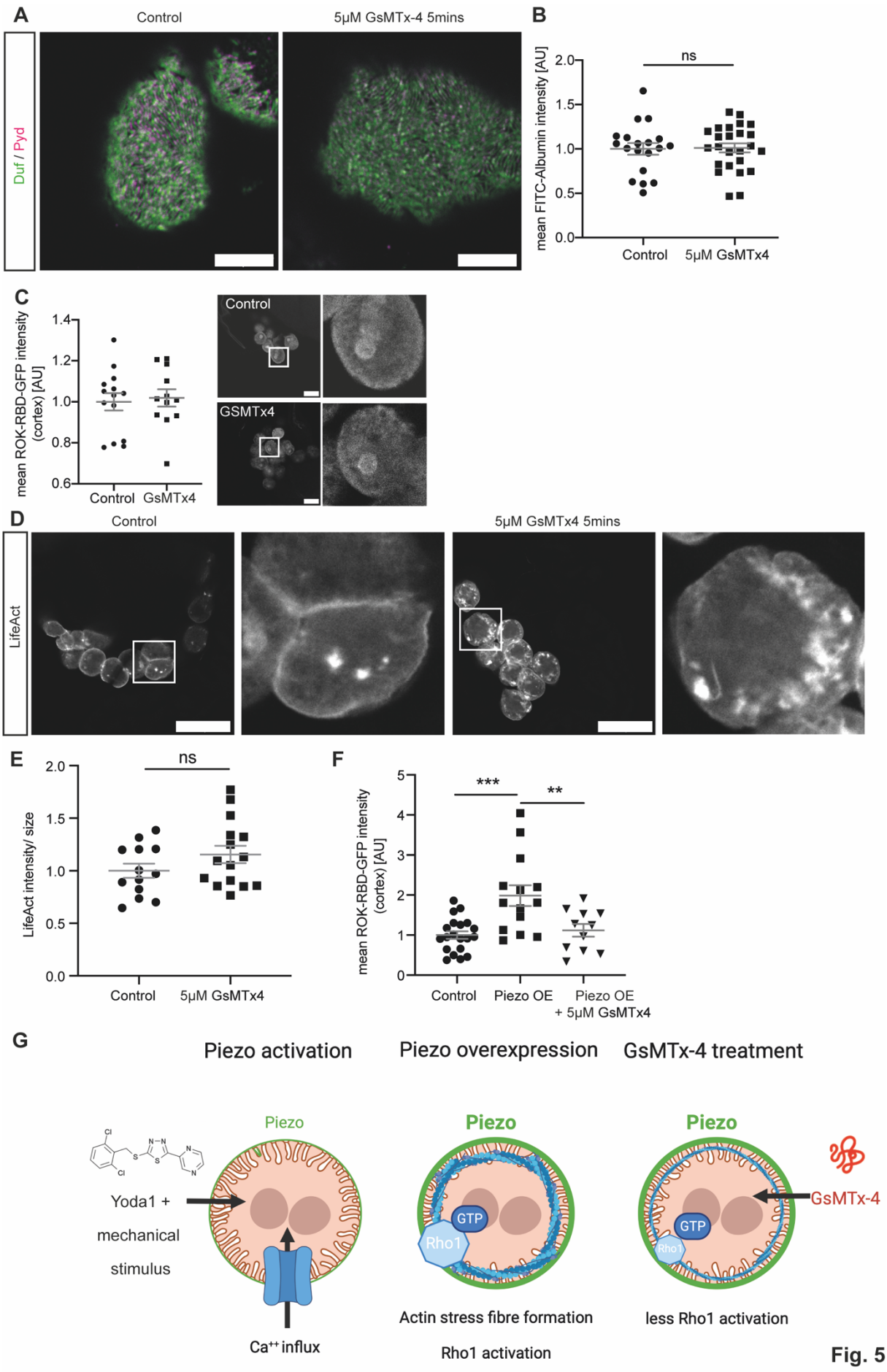
A
Control
5μM GsMTx-4 5mins
Duf / Pyd
B
ns
mean FITC-Albumin intensity [AU]
2.0
1.5
1.0
0.5
0.0
Control
5μM GsMTx4
C
mean ROK-RBD-GFP intensity (cortex) [AU]
1.4
1.2
1.0
0.8
0.6
Control
GsMTx4
Control
GSMTx4
D
Control
5μM GsMTx4 5mins
LifeAct
E
ns
LifeAct intensity/ size
2.0
1.5
1.0
0.5
0.0
Control
5μM GsMTx4
F
***
**
mean ROK-RBD-GFP intensity (cortex) [AU]
5
4
3
2
1
0
Control
Piezo OE
Piezo OE + 5μM GsMTx4
G
Piezo activation
Piezo overexpression
GsMTx-4 treatment
Piezo
Yoda1 +
mechanical
stimulus
Ca++ influx
Piezo
GTP
Rho1
Actin stress fibre formation
Rho1 activation
Piezo
GTP
Rho1
GsMTx-4
less Rho1 activation

Fig. 5

1

Figure 5: GsMTx4 treatment did not result in a nephrocyte phenotype and reduced elevated Rho1 activity levels in Piezo overexpression cells. A Immunofluorescence staining with Duf and Pyd antibodies did not reveal any morphological changes after incubation with 5μM GsMTx4 for 5 min. Scale bar = 5 μm. **B** FITC-Albumin binding assays did not reveal any differences between controls and nephrocytes incubated with GsMTx4 for 5 min. **C** Quantification of GTPase activity levels at the cell cortex did not reveal any changes in Rho1-GTP (Rok-RBD-GFP) levels. Scale bar = 25 μm. Rok-GFP: w; *sns*-Gal4/+;UAS-*dicer2*/UAS-*rok-RBD*-GFP. **D,E** Visualization of the actin cytoskeleton did not show a significant increase of actin clusters after incubation of nephrocytes with GsMTx4 for 5 min. Scale bar = 50 μm. w; *sns*-Gal4/+;UAS-*dicer2*/UAS-*LifeACT*-RFP. **F** GTP-bound Rho1 levels were significantly reduced at the cell cortex in Piezo overexpressing cells (w; *sns*-Gal4/+; UAS-*rok-RBD*-GFP/UAS-*Piezo*-GFP) after 5 min treatment with GsMTx4, when compared to untreated Piezo wildtype overexpressing cells. Comparison with control cells revealed no significant change of Rho1-GTP levels at the cortex in Piezo overexpressing cells treated with GsMTx4 (w; *sns*-Gal4/+; UAS-*rok-RBD*-GFP/+). 1-Way ANOVA with Tukey's multiple comparison test: **: $p < 0.01$; ***: $p < 0.001$. **G** Piezo localizes to the cell cortex, close to the nephrocyte diaphragm protein Duf and Pyd. Activation of the channel with its agonist Yoda1 results in an increased Ca^{++} influx after applying mechanical force (left panel). Elevated Piezo levels have a pathological effect on nephrocyte biology and cause a severe nephrocyte phenotype. Elevated Piezo levels also result in activation of Rho1 and an increased formation of cortical actin stress fibres and actin clusters (middle panel). Treatment with the antagonist GsMTx4, tarantula toxin, significantly reduced the elevated Rho1-GTP levels upon increased Piezo levels, exhibiting a potential as a future therapeutic (right panel). Images created with BioRender.com.

Discussion

Mechanotransducers play a crucial role in podocyte biology and within this study, we were able to delineate the physiological role of the mechanosensitive ion channel Piezo in nephrocytes for the first time. Here, we provide evidence that Piezo is expressed at the nephrocyte diaphragm. Our data shows that Piezo wildtype overexpression caused altered Ca^{++} signalling, Rho1 hyperactivity at the cell cortex and actin stress fibre and actin cluster formation in nephrocytes. Moreover, an increase in Piezo wildtype protein levels resulted in morphological and functional disturbances in nephrocytes **(Figure 5G)**. The expression of a mutant variant of Piezo, lacking the mechanosensitive channel activity did not cause morphological and functional disturbances, altered Ca^{++} signalling and also did not impact on Rho1 activation, suggesting the observed phenotype is mediated via the mechanosensitive function of Piezo.

Within this study, we performed Ca^{++} imaging in isolated pericardial cells from adult flies and could show an increase of intracellular Ca^{++} levels after applying mechanical force and pre-treatment with Yoda1, a Piezo agonist. Interestingly, overexpression of Piezo wildtype resulted in an oscillating pattern of Ca^{++}, which was less observed in controls or cells expressing the mutant variant of Piezo. Our data suggests an opening of the channel upon a mechanical stimulus (puff), which is facilitated after binding of Yoda1 between the Arm domain and the repeat A [30]. The increased number of channels seem to be causative for the constitutive oscillating pattern in the majority of flies overexpressing Piezo wildtype. Whether the overexpression also impacts on channel activity is unknown. Inhibiting mechanosensitive channel activity of Piezo abolished the oscillating pattern, implying that the oscillation is caused by the mechanosensitive channel activity and that elevated Piezo wildtype levels sense mechanical stress during our experiment, causing Ca^{++} influx.

In a recent study, Sivakumar et al. showed that nephrocytes exhibit stochastic Ca^{++} waves *in vivo* [44]. They were also able to show a functional role of store operated Ca^{++} entry (SOCE) mechanisms, in particular Stim and Orai-dependent, on nephrocyte endocytosis [44]. Thus, this data, together with the data provided in here, show that Ca^{++} signalling is an important signalling feature in *Drosophila* nephrocytes.

The tight regulation of GTPases is essential to maintain podocyte health and survival. Previous studies revealed a pathological effect of overactive RhoA and Rac1 in mice. This includes albuminuria as well as foot process effacement and the activation of both GTPases is associated with FSGS and minimal change disease [36–38]. Here, we identified increased Rho1 activity levels at the cell cortex after overexpression of Piezo wildtype. Interestingly, overexpression of a Piezo mutant, lacking mechanosensitive channel activity, did not cause elevated Rho1 activity levels

at the cell cortex, suggesting the Rho1 activation is dependent on the mechanosensitive function of Piezo. Further, FITC-Albumin binding disturbances observed in Piezo wildtype overexpressing nephrocytes, were rescued by simultaneous expression of a dominant-negative variant of Rho1. The data imply, that activation of Rho1 might mediate, at least in part, the nephrocyte phenotype associated with Piezo hyperactivity, including morphological and functional disturbances.

Mechanosensors, such as TRP channels, also have been described to regulate GTPase activation in podocytes [45]. One downstream target of GTPases is the actin cytoskeleton, which plays an essential role during podocyte injury and rearrangement processes [46]. Here, we show that chronic elevation of Piezo wildtype results in an increase of actin stress fibres. In cultured podocytes, the expression of over-active RhoA (Rho1 in *Drosophila*) caused a significant increase of actin stress fibres [39], a similar effect to what we observed in the Piezo wildtype overexpression nephrocytes, strengthening the link between Piezo, Ca^{++} signalling, Rho1 activation and the actin cytoskeleton.

Our findings, that GTPase activation and subsequent actin stress fibre formation have relevance to podocytes response to injury, are supported by a previous study investigating the effect of Bis-T-23 in podocytes. Bis-T-23 promotes actin-dependent dynamin oligomerization and stabilizes the actin cytoskeleton during podocyte injury [47]. In detail, several injury models which caused actin-cytoskeleton rearrangement could be at least partially rescued by Bis-T-23 treatment, again emphasising the importance of the actin-cytoskeleton and upstream regulators such as GTPases [47].

Assuming a correlation between over-active Piezo variants and a glomerular disease phenotype, a treatment to block Piezo activation could be beneficial for patients. Our data showed that the treatment with tarantula toxin (GsMTx4) was able to significantly reduce the increased Rho1-GTP levels at the cell cortex in nephrocytes

overexpressing Piezo wildtype. Interestingly, GsMTx4 is currently used in clinical trials as a novel treatment for muscle dystrophy (https://laforcedmd.com/tarantula-venom-dmd/) and would therefore be an ideal candidate for patients suffering from Piezo over-activation induced glomerular disease. In addition, a recent study investigated the association between Piezo1 activation and kidney fibrosis [48]. Tubular Piezo1 was increased in fibrotic kidneys and inhibition of Piezo1 with GsMTx4 resulted in attenuated tubulointerstitial fibrosis [48], further supporting the idea of GsMTx4 use as a potential intervention in the future.

Taken together, here we provide evidence that the mechanosensitive ion channel Piezo is localizing to the nephrocyte diaphragm, that it regulates Rho1 activity levels and the formation of actin stress fibres, and that Piezo activity levels require to be tightly regulated to maintain normal nephrocyte morphology and function.

1 **Material and Methods**

2 **Table 1: List of antibodies**

Name	Company/ Provider	Catalog nr. / Reference	Host Species	Dilution IF
Albumin	Abcam	ab207327	Rabbit	1:25
Duf	M. Ruiz-Gomez	[26]	Rabbit	1:100
Pyd	Developmental Studies Hybridoma Bank	PYD2	Mouse	1:25
Piezo1	Novus Biologicals	NBP1-78537-0.025ml	Rabbit	1:25
Synaptopodin	Synaptic Systems	163 004	Guinea Pig	1:200

3

4 **Table 2: List of fly strains**

Fly strain	Origin	Purpose	Chromosome
Piezo MI{MIC}	BDSC ID: 60209	Endogenous GFP-tag	2. Chr.
Piezo^{ko}	BDSC ID: 58770	Knockout	2. Chr.
UAS-*piezo*-GFP	BDSC ID: 58773	Overexpression	3. Chr.
UAS-*piezo*-flag	BDSC ID: 95296	Overexpression	3. Chr.
UAS-*piezo*.2306MYC.flag	BDSC ID: 95298	Overexpression	3. Chr.

UAS-*piezo*-RNAi	VDRC ID: 101915	Knockdown	2. Chr.
sns-Gal4; UAS-*dicer*2	the *sns*-Gal4 strain was obtained from S. Abmayr [49] and combined with UAS-*dicer2* [8]	Nephrocyte-specific driver	2. + 3. Chr.
UAS-Rok-RBD-GFP	BDSC ID: 52290	Rho1 sensor	3. Chr.
UAS-Rho1.N19	BDSC ID: 7328	dominant-negative Rho1	3. Chr.
UAS-LifeAct-RFP	BDSC ID: 58362	Overexpression	3. Chr.
UAS-GCaMP6medium	BDSC ID: 42750	Overexpression	3. Chr.
Oregon R		wildtype	
W^{1118}		wildtype	

Fly husbandry and generation

For experiments all flies were kept at 25°C or 28°C. The nephrocyte-specific knockdown or overexpression was achieved by mating UAS fly strains with the *sns*-Gal4 strain.

Yoda1 and GsMTx4 treatment

To activate Piezo acutely, nephrocyte were incubated with the specific activator compound Yoda1 (30μm in DMSO; control: DMSO) (Sigma, now Merck). To inhibit mechanosensitive channel activity in an unspecific way, nephrocytes were incubated

with tarantula toxin/GsMTx4 (5μM in H_2O; control: HL3 buffer) (Alomone labs, Jerusalem, Israel, Cat. nr: STG-100). For all experiments nephrocytes were isolated as described below in haemolymph-like buffer (HL3.1; 70 mM NaCl, 5 mM KCl, 1.5 mM $CaCl_2$, 4 mM $MgCl_2$, 10 mM $NaHCO_3$, 115 mM Sucrose and 5 mM Hepes). Cells were then incubated for 5 mins followed by a washing step in HL3.1 for one min.

Immunofluorescences of *Drosophila* tissue

Garland nephrocytes were isolated from 3rd instar larvae in HL3.1 buffer. For isolation of pericardial cells, the cuticle of the abdomen of 1-3 days old flies was dissected and pericardial cells were still attached to the heart tube. The whole tissue was used for immunofluorescence stainings and the dissection was performed in HL3.1 buffer. After isolation cells were fixed in 4 % formaldehyde for 20 mins, followed by three washing steps with washing buffer (Phosphate buffer saline, 0.5% bovine serum albumin, 0.03% Triton-X) for 20 mins. Primary antibody incubation was done overnight at 4°C. On day 2, the cells were washed three times for 20 mins, incubated with 5 % normal horse serum for 30 min and 1 h with the respective secondary antibody. Afterwards followed three washing steps for 20 mins and mounting with mounting medium (2.5% propyl gallate and 85% glycerol). Imaging was done using either a Zeiss LSM 8 confocal combined with an Airyscan for higher resolution or a Leica SP8 confocal. Images were further processed using ImageJ (version 1.53c).

For co-localization studies we used the JACoP plugin from S. Bolte and F.P. Cordelières [50]. This Fiji plugin calculates the Pearson's correlation coefficient. We measured the co-localisation of Duf with Piezo:GFP and Pyd with Piezo:GFP and depicted the Pearson's coefficient for the different cell types. To quantify nephrocyte density (nephrocyte diaphragm length [$\mu m/\mu m^2$]) we used our previously published macro for FIJI, which was adapted for Airyscan confocal images [51]. Graphs depict

single nephrocytes, which were isolated from three to seven individual animals from independent matings.

Immunofluorescence of murine tissue

Paraffin-embedded tissue from wildtype mice was used for immunofluorescence stainings. Tissue was de-paraffinized by passing through a descending alcohol row. After washing for three times (5 mins) with H_2O followed by three washing steps with Dako wash buffer (Agilent Technologies, Santa Clara, USA), antigen retrieval was done in a steamer using pH9 antigen retrieval from Dako. Primary antibodies (listed in Table 1) were diluted in Dako antibody diluent and incubated overnight at 4°C. The next day sections were washed for three times (5 mins) with Dako wash buffer, followed by secondary antibody incubation with DAPI for one hour at room temperature. Prior to mounting with Prolong Gold, samples were again washed for three times. Imaging of samples was done at a Zeiss LSM 900 confocal combined with Airyscan. Images were further processed using ImageJ (version 1.53c).

FITC-Albumin binding assay

FITC-Albumin binding assays were performed as previously published [8,52]. Garland nephrocytes were isolated from 3rd instar larvae and incubated with FITC-Albumin (0,2 mg/ml; Sigma-Aldrich, St. Louis, USA) for 1 min, followed by 20 mins fixation with 4 % Formaldehyde. For UAS-Piezo-GFP expressing nephrocytes an anti-Albumin antibody was used to label albumin with Cy3 for quantification. Imaging was done with a Zeiss LSM 5 confocal or Leica SP8 confocal microscope and images were further processed and analysed using ImageJ (version 1.53c). For comparative analysis, the exposure time of experiments was kept identical. The mean intensity of FITC-Albumin was measured and normalized to control cells.

$AgNO_3$ toxin assay

Flies of the appropriate genotype were allowed to lay eggs for 24 hrs at 25°C on juice plates with normal yeast. Afterwards, plates with eggs were kept at 18°C for 24 hrs. 1st instar larvae were then transferred to juice plates supplemented with yeast paste containing $AgNO_3$ (2 g yeast in 3.5 ml 0.003% $AgNO_3$). Plates were kept at 25°C for 4 days to let larvae develop and pupate. 5 days after egg laying pupae were counted daily for 4 consecutive days. The number of pupae was normalized to the number of 1st instar larvae transferred to the plates.

Quantification of GTPase activity levels

To quantify activity levels of Rho1 in garland nephrocytes UAS-Rok-RBD-GFP flies were combined with the nephrocyte-specific driver *sns*-Gal4. For final matings, these flies were either combined with UAS-*piezo*.flag or UAS-*piezo*.2306MYC.flag flies. Garland nephrocytes from 3rd instar larvae were isolated and fixed for 20 mins with 4 % formaldehyde followed by mounting with mounting medium. Images were obtained using a Leica SP8 confocal or Zeiss LSM 900 confocal and further image processing was done using ImageJ (version 1.53c). For comparative analysis, laser intensity and settings were kept equal. Quantification was done using the brush selection tool from FIJI to only measure GFP intensity at the cell cortex, where activated GTPases seem to localize.

Visualization of the actin filaments

For actin cytoskeleton visualization, the nephrocyte-specific driver *sns*-Gal4, UAS-LifeAct-RFP and UAS-Piezo-GFP flies were combined. Garland nephrocytes were isolated from 3rd instar larvae and fixed for 20 mins with 4 % Formaldehyde, prior to mounting with mounting medium. Images were obtained using a Leica SP8 confocal.

Further image processing was done using ImageJ (version 1.53c). For quantification mean intensities of RFP were measured and normalized to cell size. For comparative analysis, laser intensity and settings were kept equal.

Ca^{++} imaging of pericardial nephrocytes

For Ca^{++} imaging purposes, UAS-GCaMP6 flies were combined with the nephrocyte-driver *sns*-Gal4 and mated with UAS-*piezo*.flag or UAS-*piezo*.2306MYC.flag to obtain experimental animals. Flies were kept at 25°C until the experimental flies were 1-5 days old. Flies were anesthetized with Flynap (Carolina Biological Supply company, North Carolina, USA). Pericardial nephrocytes were isolated but still attached to the heart tube and the cuticle. The tissue was kept in HL3.1 buffer at room temperature. For Yoda1 treatment, the tissue was incubated with 30 μM Yoda1 dissolved in DMSO or DMSO (control) for 5 mins prior to measurements. The tissue was glued onto coverslips with vaseline, transferred into a recording chamber filled with either 1 mL Yoda1 (30 μM) in HL3.1 buffer, DMSO (equal amount to Yoda1) in HL3.1 buffer or HL3.1 buffer (Piezo flies) as bath solution, and secured with a platinum grid. GCaMP6 was excited at 488 nm, and fluorescence was collected between 500 and 530 nm using a confocal microscope (eC1, Nikon, Düsseldorf, Germany). Time series of images were recorded at a rate of 1 frame every second. To apply a pressure stimulus, a glass micropipette (GC150TF-10, Harvard Apparatus, USA) was pulled with a patch-pipette puller (Flaming/Brown P97, Sutter Instruments, Novato, CA, USA) with an electrical resistance of 200-300 kΩ. The micropipette was either filled with Yoda1 (30 μM), DMSO (equal amount to Yoda1) or HL3.1 buffer and positioned on the bath solution's surface. GCaMP6 baseline fluorescence was recorded for 60 secs, followed by pressure-controlled release of the pipette solution (referred to as ‘puff’, 0.2 bar for 3 secs, PDES-01 a.m., NPI electronic GmbH, Tamm, Germany). GCaMP6 fluorescence

was recorded after the puff for another 340 secs. Data were evaluated with Nikon EZ-C1 Viewer (Nikon), processed using Excel (Microsoft, USA), and statistical tests were applied with Graph Pad Prism software. GCaMP6-expressing nephrocytes were marked as a region of interest (ROI) and the mean fluorescence intensity within the ROI was measured throughout the time series. The mean fluorescence intensity (F) was normalized to the baseline fluorescence intensity before the puff (mean of 10 values prior to puff) and set to 1.0, hence changes in fluorescence intensity are stated as ΔF/F. Quantification of Ca^{++} transients was achieved by calculating the maximum increase of GCaMP6 intensity after the puff within 25 secs after puff. The number of experiments is given as n, whereas n represents the averaged values of all ROIs analysed in one fly. Traces of calcium signals were created with OriginPro 9.1G (OriginLab Corporation, USA) and composed using Adobe Illustrator and Adobe Photoshop (Adobe Systems Software, Ireland). Visualizations of changes in fluorescence were created using Fiji ImageJ (National Institutes of Health, USA) and composed with Adobe Photoshop (Adobe Systems Software, Ireland). In these visualizations, red signals indicate the difference between baseline brightness and brightness at the indicated timeslots.

Transcriptomic data analysis

Publicly available murine [34] und human single nucleus RNA-sequencing (snRNAseq) and ATAC-seq [35] data have been searched for Piezo1 expression. Data and analyser have been used provided by KIT (kidney interactive transcriptomics) http://humphreyslab.com/SingleCell/. Permission to use the graphs generated has been provided by Benjamin Humphreys. In addition, human single cell RNA-sequencing data (scRNAseq) provided by the Kidney Precision Medicine Project (KPMP) consortium have been searched for Piezo1 expression. The results here are

in whole or part based upon data generated by the Kidney Precision Medicine Project. Accessed November 14th, 2023. https://www.kpmp.org. Funded by the National Institute of Diabetes and Digestive and Kidney Diseases (Grant numbers: U01DK133081, U01DK133091, U01DK133092, U01DK133093, U01DK133095, U01DK133097, U01DK114866, U01DK114908, U01DK133090, U01DK133113, U01DK133766, U01DK133768, U01DK114907, U01DK114920, U01DK114923, U01DK114933, U24DK114886, UH3DK114926, UH3DK114861, UH3DK114915, UH3DK114937)

Statistical analysis

To determine statistical significance Graph Pad Prism software version 8 for Mac (GraphPad Software, San Diego, CA) was used. All results are expressed as means ± SEM. Datapoints represent single flies from independent matings, if not stated differently. Comparison of two groups was done using a student's t-test. A *P-value* < 0.05 was considered statistically significant. Comparison of more than two groups with one independent variable was done using one-way ANOVA followed by Tukey's multiple comparisons test. A *P-value* < 0.05 was considered statistically significant.

Data Availability Statement

Data sharing not applicable as no datasets were generated during this study.

Conflict of Interest Statement

The authors declare no conflicts of interest.

Author contribution

S.K. conceived the study, made the figures and drafted the paper, K.S., I.E. and S.K. performed experiments, S.K., M.L. and K.S. analysed data, B.D., C.L. and T.B.H. revised the study critically for important intellectual content, S.K. and B.D. revised the paper; all authors approved the final version of the manuscript.

Acknowledgement

The Anti-Pyd monoclonal antibody developed by Fanning [53] was obtained from the Developmental Studies Hybridoma Bank, created by the NICHD of the NIH and maintained at The University of Iowa, Department of Biology, Iowa City, IA 52242. Images were created with BioRender.com.

Funding

S.K. received funding from the German Research Foundation (KO 6045/1-1 and KO 6045/4-1). T.B.H. received funding from the German Research Foundation (CRC1192, HU 1016/8-2, HU 1016/11-1, HU 1016/ 12-1). S.K. and T.B.H received funding from the BMBF (STOP-FSGS- 01GM1901C).

Conflict of Interest

None. The authors have nothing to disclose.

References

1. Pavenstädt, H., Kriz, W. & Kretzler, M. Cell biology of the glomerular podocyte. *Physiol. Rev.* **83**, 253–307 (2003).
2. Kestilä, M. *et al.* Positionally cloned gene for a novel glomerular protein--nephrin--is mutated in congenital nephrotic syndrome. *Mol. Cell* **1**, 575–582 (1998).
3. Boute, N. *et al.* NPHS2, encoding the glomerular protein podocin, is mutated in autosomal recessive steroid-resistant nephrotic syndrome. *Nat. Genet.* **24**, 349–354 (2000).
4. Kaplan, J. M. *et al.* Mutations in ACTN4, encoding alpha-actinin-4, cause familial

focal segmental glomerulosclerosis. *Nat. Genet.* **24**, 251–256 (2000).
5. Winn, M. P. *et al.* A mutation in the TRPC6 cation channel causes familial focal segmental glomerulosclerosis. *Science* **308**, 1801–1804 (2005).
6. Hildebrandt, F. Genetic kidney diseases. *Lancet Lond. Engl.* **375**, 1287–1295 (2010).
7. Markowitz, G. S., Bomback, A. S. & Perazella, M. A. Drug-Induced Glomerular Disease: Direct Cellular Injury. *Clin. J. Am. Soc. Nephrol.* **10**, 1291–1299 (2015).
8. Koehler, S. *et al.* Proteome Analysis of Isolated Podocytes Reveals Stress Responses in Glomerular Sclerosis. *J. Am. Soc. Nephrol. JASN* **31**, 544–559 (2020).
9. Greiten, J. K. *et al.* The role of filamins in mechanically stressed podocytes. *FASEB J. Off. Publ. Fed. Am. Soc. Exp. Biol.* **35**, e21560 (2021).
10. Feng, D., DuMontier, C. & Pollak, M. R. Mechanical challenges and cytoskeletal impairments in focal segmental glomerulosclerosis. *Am. J. Physiol. - Ren. Physiol.* **314**, F921–F925 (2018).
11. Endlich, N. *et al.* Podocytes respond to mechanical stress in vitro. *J. Am. Soc. Nephrol. JASN* **12**, 413–422 (2001).
12. Endlich, K., Kliewe, F. & Endlich, N. Stressed podocytes-mechanical forces, sensors, signaling and response. *Pflugers Arch.* **469**, 937–949 (2017).
13. Kriz, W. & Lemley, K. V. Mechanical challenges to the glomerular filtration barrier: adaptations and pathway to sclerosis. *Pediatr. Nephrol.* **32**, 405–417 (2017).
14. Kriz, W. & Lemley, K. V. A Potential Role for Mechanical Forces in the Detachment of Podocytes and the Progression of CKD. *J. Am. Soc. Nephrol.* **26**, 258–269 (2015).
15. Wiggins, J. E. *et al.* Podocyte hypertrophy, 'adaptation,' and 'decompensation' associated with glomerular enlargement and glomerulosclerosis in the aging rat: prevention by calorie restriction. *J. Am. Soc. Nephrol. JASN* **16**, 2953–2966 (2005).
16. Rinschen, M. M. *et al.* YAP-mediated mechanotransduction determines the podocyte's response to damage. *Sci. Signal.* **10**, (2017).
17. Tian, X. *et al.* Podocyte-associated talin1 is critical for glomerular filtration barrier maintenance. *J. Clin. Invest.* **124**, 1098–1113 (2014).
18. Okabe, M. *et al.* Indirect podocyte injury manifested in a partial podocytectomy mouse model. *Am. J. Physiol. Renal Physiol.* (2021) doi:10.1152/ajprenal.00602.2020.
19. Dalghi, M. G. *et al.* Expression and distribution of PIEZO1 in the mouse urinary tract. *Am. J. Physiol.-Ren. Physiol.* **317**, F303–F321 (2019).
20. Coste, B. *et al.* Piezo1 and Piezo2 are essential components of distinct mechanically activated cation channels. *Science* **330**, 55–60 (2010).
21. Coste, B. *et al.* Piezo proteins are pore-forming subunits of mechanically activated channels. *Nature* **483**, 176–181 (2012).
22. Cahalan, S. M. *et al.* Piezo1 links mechanical forces to red blood cell volume. *eLife* **4**, (2015).
23. Ranade, S. S. *et al.* Piezo1, a mechanically activated ion channel, is required for vascular development in mice. *Proc. Natl. Acad. Sci. U. S. A.* **111**, 10347–10352 (2014).
24. Retailleau, K. *et al.* Piezo1 in Smooth Muscle Cells Is Involved in Hypertension-Dependent Arterial Remodeling. *Cell Rep.* **13**, 1161–1171 (2015).
25. Zhong, M., Komarova, Y., Rehman, J. & Malik, A. B. Mechanosensing Piezo channels in tissue homeostasis including their role in lungs. *Pulm. Circ.* **8**, 2045894018767393 (2018).
26. Weavers, H. *et al.* The insect nephrocyte is a podocyte-like cell with a filtration slit diaphragm. *Nature* **457**, 322–326 (2009).
27. Zhuang, S. *et al.* Sns and Kirre, the Drosophila orthologs of Nephrin and Neph1, direct adhesion, fusion and formation of a slit diaphragm-like structure in insect nephrocytes. *Dev. Camb. Engl.* **136**, 2335–2344 (2009).
28. Akoglu, H. User's guide to correlation coefficients. *Turk. J. Emerg. Med.* **18**, 91–93

(2018).
29. Syeda, R. *et al.* Chemical activation of the mechanotransduction channel Piezo1. *eLife* **4**, (2015).
30. Botello-Smith, W. M. *et al.* A mechanism for the activation of the mechanosensitive Piezo1 channel by the small molecule Yoda1. *Nat. Commun.* **10**, 4503 (2019).
31. Hill, R. Z. *et al. Renal mechanotransduction is an essential regulator of renin*. http://biorxiv.org/lookup/doi/10.1101/2023.11.04.565646 (2023) doi:10.1101/2023.11.04.565646.
32. Liu, S. *et al.* Single-cell transcriptomics reveals a mechanosensitive injury signaling pathway in early diabetic nephropathy. *Genome Med.* **15**, 2 (2023).
33. Rinschen, M. M. *et al.* A Multi-layered Quantitative In Vivo Expression Atlas of the Podocyte Unravels Kidney Disease Candidate Genes. *Cell Rep.* **23**, 2495–2508 (2018).
34. Wu, H. *et al.* Mapping the single-cell transcriptomic response of murine diabetic kidney disease to therapies. *Cell Metab.* **34**, 1064-1078.e6 (2022).
35. Wilson, P. C. *et al.* Multimodal single cell sequencing implicates chromatin accessibility and genetic background in diabetic kidney disease progression. *Nat. Commun.* **13**, 5253 (2022).
36. Zhu, L., Jiang, R., Aoudjit, L., Jones, N. & Takano, T. Activation of RhoA in podocytes induces focal segmental glomerulosclerosis. *J. Am. Soc. Nephrol. JASN* **22**, 1621–1630 (2011).
37. Yu, H. *et al.* Rac1 activation in podocytes induces rapid foot process effacement and proteinuria. *Mol. Cell. Biol.* **33**, 4755–4764 (2013).
38. Robins, R. *et al.* Rac1 activation in podocytes induces the spectrum of nephrotic syndrome. *Kidney Int.* **92**, 349–364 (2017).
39. Wang, L. *et al.* Mechanisms of the proteinuria induced by Rho GTPases. *Kidney Int.* **81**, 1075–1085 (2012).
40. Muraleedharan, S., Sam, A., Skaer, H. & Inamdar, M. S. Networks that link cytoskeletal regulators and diaphragm proteins underpin filtration function in Drosophila nephrocytes. *Exp. Cell Res.* **364**, 234–242 (2018).
41. Zhang, Y. *et al.* Piezo1-Mediated Mechanotransduction Promotes Cardiac Hypertrophy by Impairing Calcium Homeostasis to Activate Calpain/Calcineurin Signaling. *Hypertension* **78**, 647–660 (2021).
42. Xie, Q. *et al.* Transcription factor Acj6 controls dendrite targeting via a combinatorial cell-surface code. *Neuron* **110**, 2299-2314.e8 (2022).
43. Suchyna, T. M. *et al.* Identification of a peptide toxin from Grammostola spatulata spider venom that blocks cation-selective stretch-activated channels. *J. Gen. Physiol.* **115**, 583–598 (2000).
44. Sivakumar, S., Miellet, S., Clarke, C. & Hartley, P. S. Insect nephrocyte function is regulated by a store operated calcium entry mechanism controlling endocytosis and Amnionless turnover. *J. Insect Physiol.* **143**, 104453 (2022).
45. Tian, D. *et al.* Antagonistic regulation of actin dynamics and cell motility by TRPC5 and TRPC6 channels. *Sci. Signal.* **3**, ra77 (2010).
46. Wang, Q. *et al.* Role of Transient Receptor Potential Canonical Channel 6 (TRPC6) in Diabetic Kidney Disease by Regulating Podocyte Actin Cytoskeleton Rearrangement. *J. Diabetes Res.* **2020**, (2020).
47. Schiffer, M. *et al.* Pharmacological targeting of actin-dependent dynamin oligomerization ameliorates chronic kidney disease in diverse animal models. *Nat. Med.* **21**, 601–609 (2015).
48. Zhao, X. *et al.* Mechanosensitive Piezo1 channels mediate renal fibrosis. *JCI Insight* **7**, e152330 (2022).
49. Kocherlakota, K. S., Wu, J., McDermott, J. & Abmayr, S. M. Analysis of the Cell

Adhesion Molecule Sticks-and-Stones Reveals Multiple Redundant Functional Domains, Protein-Interaction Motifs and Phosphorylated Tyrosines That Direct Myoblast Fusion in *Drosophila melanogaster*. *Genetics* **178**, 1371–1383 (2008).

50. Bolte, S. & Cordelières, F. P. A guided tour into subcellular colocalization analysis in light microscopy. *J. Microsc.* **224**, 213–232 (2006).

51. Koehler, S. *et al.* Scaffold polarity proteins Par3A and Par3B share redundant functions while Par3B acts independent of atypical protein kinase C/Par6 in podocytes to maintain the kidney filtration barrier. *Kidney Int.* S0085-2538(21)01150–9 (2021) doi:10.1016/j.kint.2021.11.030.

52. Hermle, T., Braun, D. A., Helmstädter, M., Huber, T. B. & Hildebrandt, F. Modeling Monogenic Human Nephrotic Syndrome in the Drosophila Garland Cell Nephrocyte. *J. Am. Soc. Nephrol. JASN* **28**, 1521–1533 (2017).

53. Choi, W. *et al.* The single Drosophila ZO-1 protein Polychaetoid regulates embryonic morphogenesis in coordination with Canoe/afadin and Enabled. *Mol. Biol. Cell* **22**, 2010–2030 (2011).